

AD-A053 553

COLORADO STATE UNIV FORT COLLINS DEPT OF CHEMISTRY  
ABSORPTION AND ELECTRONIC RAMAN SCATTERING SPECTRA OF THE GAMMA--ETC(U)  
MAR 78 E R BERNSTEIN, J D WEBB  
TR-17

F/G 7/4

N00014-75-C-1179

NL

UNCLASSIFIED

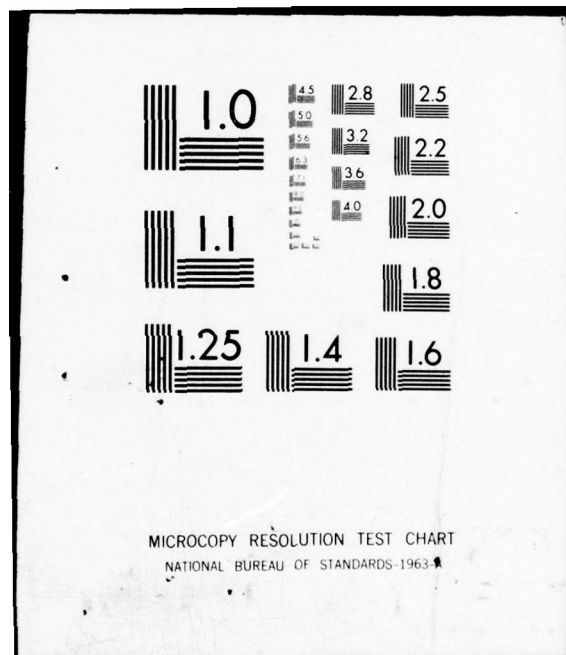
1 OF 1

AD  
A053 553



END  
DATE  
FILMED  
6-78

DDC



AD A 053553

AD NO. 1  
DDC FILE COPY

OFFICE OF NAVAL RESEARCH

Contract N00014-75-C-1179

Task No. NR 056-607

TECHNICAL REPORT NO. 17

12

"ABSORPTION AND ELECTRONIC RAMAN SCATTERING SPECTRA OF  
THE  $\Gamma_{8g}$  ( $^2T_{1g}$ ) STATE OF  $\text{IrF}_6$  AT  $1.6\mu$  - A RESOLUTION  
OF THE JAHN-TELLER PROBLEM"

by

E. R. Bernstein and J. D. Webb

Prepared for Publication  
in  
Molecular Physics

Department of Chemistry  
Colorado State University  
Fort Collins, Colorado 80523

March 1978

Reproduction in whole or in part is permitted for  
any purpose of the United States Government.

Approved for Public Release; Distribution Unlimited.

DDC  
RECEIVED  
MAY 4 1978  
D

UNCLASSIFIED

SECURITY CLASSIFICATION OF THIS PAGE (When Data Entered)

REPORT DOCUMENTATION PAGE		READ INSTRUCTIONS BEFORE COMPLETING FORM
1. REPORT NUMBER (14) TR-17	2. GOVT ACCESSION NO.	3. RECIPIENT'S CATALOG NUMBER
4. TITLE (and Subtitle) (6) Absorption and Electronic Raman Scattering Spectra of the $T_{8g}$ State of $IrF_6$ at $1.6\mu$ - A Resolution of the Jahn-Teller Problem. <i>micrometers</i>		5. TYPE OF REPORT & PERIOD COVERED (7) Technical Report
7. AUTHOR(s) (10) E. R./Bernstein J. D./Webb <i>Gamma sub 8g</i>		6. PERFORMING ORG. REPORT NUMBER CONTRACT OR GRANT NUMBER(s) N00014-75-C-1179
9. PERFORMING ORGANIZATION NAME AND ADDRESS Department of Chemistry Colorado State University Fort Collins, Colorado 80523		10. PROGRAM ELEMENT, PROJECT, TASK AREA & WORK UNIT NUMBERS NR 056-607
11. CONTROLLING OFFICE NAME AND ADDRESS Office of Naval Research Arlington, VA 22217		12. REPORT DATE (11) Mar 1978
14. MONITORING AGENCY NAME & ADDRESS (if different from Controlling Office)		13. NUMBER OF PAGES 36 (12) 35p.
		15. SECURITY CLASS. (of this report) Unclassified
		15a. DECLASSIFICATION/DOWNGRADING SCHEDULE
16. DISTRIBUTION STATEMENT (of this Report)  Approved for Public Release; Distribution Unlimited.		
17. DISTRIBUTION STATEMENT (of the abstract entered in Block 20, if different from Report)		
18. SUPPLEMENTARY NOTES		
19. KEY WORDS (Continue on reverse side if necessary and identify by block number) $IrF_6$ Electronic Raman scattering $T_{8g} (t_{2g})^3$ states Absorption spectra Jahn-Teller Effect <i>Gamma sub 8g</i> <i>sub 1g</i>		
20. ABSTRACT (Continue on reverse side if necessary and identify by block number) Electronic Raman scattering and absorption spectra are presented which allow an interpretation of the vibronic structure of the $T_{8g} ({}^2T_{1g})$ excited electronic state of $IrF_6$ at $1.6\mu$ . <i>micrometers</i> Large splittings and shifts are observed for the Jahn-Teller active $\nu_2 (e_g)$ , $\nu_5 (t_{2g})$ , and $2\nu_5$ vibrations. <i>sub 8g</i> <i>sub 2g</i> From $\rightarrow$ next page		

DD FORM 1 JAN 73 1473

EDITION OF 1 NOV 65 IS OBSOLETE  
S/N 0102-014-6601

UNCLASSIFIED

SECURITY CLASSIFICATION OF THIS PAGE (When Data Entered)

nu2

404 992

Hue

UNCLASSIFIED

SECURITY CLASSIFICATION OF THIS PAGE(When Data Entered)

20. (continued...)

these spectra linear ( $D_2^n$  and  $D_5^n$ ) and quadratic ( $Q_2^n[a_{1g}]$ ,  $Q_2^n[e_g]$ ,  $Q_5^n[a_{1g}]$ ,  $Q_5^n[e_g]$ ,  $Q_5^n[t_{2g}]$ ) Jahn-Teller parameters can be determined. These data are compared with previously obtained parameters for the  $ReF_6^n$  ground state and the  $IrF_6^n$  ( $8g$ ) ( $2T_{2g}$ ) at  $0.6\mu$ .

micrometers

Gamma sub 8g

ACCESSION for	
RTIS	White Section <input checked="" type="checkbox"/>
SEC	Buff Section <input type="checkbox"/>
UNANNOUNCED	<input type="checkbox"/>
JUSTIFICATION	
BY	
RESTRICTION/AVAILABILITY CODES	
Dist.	Avail. and/or SPECIAL
A	

## I. INTRODUCTION

This paper is one of a series in which the Jahn-Teller (JT) effect in metal hexafluorides is investigated.<sup>(1-3)</sup> The general conclusion drawn in the earlier work is that the usual linear JT theory is not an adequate one for these systems. Quadratic or higher order terms in the vibronic Hamiltonian are required. The present study of the  $\Gamma_{8g} (^2T_{1g})$  electronic state of  $\text{IrF}_6$  ( $\sim 16,400 \text{ \AA}$ ) offers an opportunity to test the generality of that conclusion and further helps to define the types of JT behavior possible for metal hexafluorides. It will be of interest, therefore, to compare and contrast the JT behavior of the  $\Gamma_{8g} (^2T_{1g})$  state with that of the  $\Gamma_{8g}$  ground state of  $\text{ReF}_6$ <sup>(1)</sup> and the  $\Gamma_{8g} (^2T_{2g})$  ( $\sim 6800 \text{ \AA}$ ) state of  $\text{IrF}_6$ .<sup>(2)</sup>

Previous work on the  $\Gamma_{8g} (^2T_{1g})$  state of neat  $\text{IrF}_6$  has been carried out;<sup>(4)</sup> however, as discussed earlier<sup>(2)</sup>, neat crystal spectra suffer from many difficulties. In the present work, better data are obtained by employing mixed crystals ( $\text{IrF}_6/\text{MoF}_6$ ). Another important experimental advantage in this present work is that both absorption and electronic Raman spectroscopy have been utilized. The concomitant differences in selection rules between the two spectroscopic techniques provides an invaluable aid in assigning the complex  $\Gamma_{8g} (^2T_{1g})$  spectrum. It might be noted that with the current availability of good photomultiplier tubes with excellent red-near IR response and high power gas and dye lasers, the usefulness of electronic Raman scattering for systems with electronic states in the IR-near IR and perhaps even the visible is much greater than its current utilization would indicate.

The theoretical and calculational methods necessary for understanding the  $\Gamma_{8g} (^2T_{1g})$  spectrum are contained in the earlier papers.<sup>(1,2)</sup> The first

paper in this series on  $\text{ReF}_6$ <sup>(1)</sup> contains a review of basic JT theory as well as discussions of the effects of low symmetry electronic crystal fields on JT systems and the importance of simultaneous treatment of the  $\nu_5$  ( $t_{2g}$ ) and  $\nu_2$  ( $e_g$ ) JT-active vibrations. Matrix elements necessary for the  $\nu_2$ - $\nu_5$  linear JT calculation are given in reference 1. A qualitative symmetry-based theory (General Vibronic Coupling-GVC) applicable to those cases in which the linear JT theory fails is also discussed in this paper. Reference 2 treats the  $\Gamma_{8g}$  ( $^2T_{2g}$ ) state of  $\text{IrF}_6$  and contains detailed information concerning the electronic, vibrational, and crystal properties of  $\text{IrF}_6$ . Linear and quadratic JT parameters are also defined and discussed in these references; the linear parameters are  $D_5$  and  $D_2$  and the quadratic ones are  $Q_5 [a_{1g}]$ ,  $Q_5 [e_g]$ ,  $Q_5 [t_{2g}]$ ,  $Q_2 [a_{1g}]$  and  $Q_2 [e_g]$ . Subscripts 5 and 2 refer to the  $\nu_5$  and  $\nu_2$  modes, respectively.

## II. EXPERIMENTAL

The two samples used in the experiment (0.5% and 5%  $\text{IrF}_6/\text{MoF}_6$ ) were prepared by previously reported methods.<sup>(5)</sup> The absorption spectra were taken at superfluid helium temperatures ( $\sim 1.6$  K) with a 1 m monochromator, a liquid nitrogen-cooled InAs infrared detector and a tungsten-iodine lamp operated at constant current. The light from the lamp was dispersed by the monochromator before impinging on the sample in order to avoid sample heating. Under these conditions the sample remained at ca. 1.5 K and the  $5\text{ cm}^{-1}$  hot band of  $\text{IrF}_6$ <sup>(2)</sup> did not congest the observed spectrum. The slitwidths used in the experiment varied from  $0.6\text{ cm}^{-1}$  up to  $1.6\text{ cm}^{-1}$  depending on line width and available intensity.

A continuous wave  $\text{Ar}^+$  pumped dye laser employing disodium fluorescein as the active medium was used to excite the electronic Raman spectrum. The available  $\text{Ar}^+$  laser lines cannot be readily employed for these experiments due to either absorption of the exciting light by the charge-transfer band ( $\sim 5000\text{ \AA}$ ) or self-absorption of the Raman scattered light by the  $\nu_{7g}$  ( $^2T_{2g}$ ) band ( $\sim 8000\text{ \AA}$ ). These problems were avoided by using either  $5400\text{ \AA}$  or  $5500\text{ \AA}$  exciting laser radiation at powers of 500 mW - 1 W. A 0.5 m double monochromator with a cooled RCA C31034A photomultiplier tube, operated in the photon counting mode, was used to detect the Raman signal. Due to the weakness of the electronic Raman signal, slitwidths had to be quite large. Most spectra were taken with slitwidths corresponding to about  $10\text{ cm}^{-1}$ . The upper wavelength limit of the photomultiplier tube ( $\sim 8500\text{ \AA}$ ) proved to be the upper limit for the electronic Raman spectrum, but since the entire fundamental region [ $\nu_{8g}$  ( $^2T_{1g}$ ) + ( $0-700\text{ cm}^{-1}$ )] was accessible, this led to no essential difficulty. Background signals were found to originate from two sources:

Pyrex glass and ice. Thus, quartz sample cells and a metal dewar with quartz windows were used, and great care was taken to exclude ice.

### III. RESULTS AND DISCUSSION

The electronic Raman and near infrared absorption data are presented in Tables 1 and 2. Some representative spectra are given in Figures 1-6.

It is helpful to discuss the selection rules and expected intensity ratios for electronic Raman scattering since the data are so important to the understanding of the complex  $\Gamma_{8g}$  ( $^2T_{1g}$ ) spectra. Koningstein<sup>(6)</sup> has shown that for non-degenerate electronic states pure electronic Raman scattering intensity is much higher than the corresponding vibronic intensity. In the case of a degenerate electronic state, however, it has been shown that the Raman intensity from the pure electronic transition can be distributed over the vibronic portion of the spectrum by a JT effect.<sup>(7)</sup> It is expected, therefore, that the Raman spectrum of the  $\Gamma_{8g}$  ( $^2T_{2g}$ ) manifold will exhibit a strong origin transition and observable  $\nu_2$  ( $e_g$ ) and  $\nu_5$  ( $t_{2g}$ ) peaks. The expectation is further strengthened by noting that if  $\text{IrF}_6$  had perfect octahedral symmetry in the  $\text{MoF}_6$  host crystal instead of only the  $C_5$  site symmetry, rigorous g-g Raman selection rule would only allow transitions to  $\{\Gamma_{8g} + (\nu_1(a_{1g}), \nu_2(e_g), \text{ or } \nu_5(t_{2g}))\}$  vibronic states. Since the crystal site effects leading to the  $C_5$  symmetry are small, it is expected that the g-g selection rule will still be approximately correct.<sup>(8)</sup> It is not clear based on these considerations whether the totally symmetric mode  $\nu_1$  should be observed.

Using the above arguments and being aware that a JT interaction might occur in the degenerate electronic state, assignment of the electronic Raman spectrum is straightforward. The crystal-field split origin (Figure 1) is easily identified by its intensity and sharpness; it is further corroborated by comparison with the absorption data (Table 2). It should be noted that the observed splitting of the origin in Raman scattering is only  $28 \text{ cm}^{-1}$  whereas

in direct absorption, the splitting is measured as  $34.6 \text{ cm}^{-1}$ . The difference,  $\sim 6 \text{ cm}^{-1}$ , is reminiscent of the ground state splitting of  $5.3 \text{ cm}^{-1}$  and suggests the following explanation: the electronic Raman sample was probably not at the bath temperature (1.6 K) due to local heating by the laser beam. Sample heating explains the observations if it is assumed that the relevant hot band transition has a greater Raman intensity than the corresponding cold transition. Five of the six observed transitions in the vibrational bending region of the spectrum ( $\Delta\sigma(\text{origin}) \sim 200 - 300 \text{ cm}^{-1}$ , see Figure 2) are assigned as vibronic components of  $\nu_5 (t_{2g})$ ; the other is  $\nu_5 (a, \text{host})$ . Similarly, four of the five peaks in the stretching region ( $600-700 \text{ cm}^{-1}$ ) are identified as  $\nu_2$  components; the remaining peak is assigned as  $\nu_3 (a, \text{host})$  (see Table 1, Figure 3, and reference 5).

The absorption data (Table 2), due to different selection rules, contain transitions other than the JT-active vibrations; these will be examined first. The  $\nu_6 (t_{2u})$  bending vibration is easily located at  $202.6 \text{ cm}^{-1}$  since this frequency is not observed in the electronic Raman spectrum and its crystal field partner is found  $34.8 \text{ cm}^{-1}$  away at  $237.4 \text{ cm}^{-1}$  (origin splitting:  $34.6 \text{ cm}^{-1}$ ). The equality of the two electronic crystal field splittings is indicative of a non-JT vibration.<sup>(1)</sup> Identification of  $\nu_4 (t_{1u})$  at  $291.1 \text{ cm}^{-1}$  is not as simple because its crystal field partner is not located at ca.  $326 \text{ cm}^{-1}$  (see Figure 4). The absence of the  $326 \text{ cm}^{-1}$  peak can, however, be rationalized if the effects of two-particle bands<sup>(2,5)</sup> are considered. It is suggested that the upper crystal field component of  $\nu_4$  has been subsumed in the  $\nu_5 (a, \text{host})$  two-particle band ( $318.4, 320.8$ , full width at half-height  $\sim 10 \text{ cm}^{-1}$ ). The intensity of this two-particle band lends credence to the conjecture, since the intensity of the transition at  $312.5 \text{ cm}^{-1}$  (a component of  $\nu_5$  which would be the most likely single particle state with which the two-particle state can mix) is not sufficient to account for the observed two-particle intensity.<sup>(5)</sup> The major

remaining non-JT-induced intensity is found at  $700.4 \text{ cm}^{-1}$  and is assigned as  $\nu_1 (a_{1g})$  rather than  $\nu_3 (t_{1u})$  because  $\nu_6 (t_{2u})$  and some  $\nu_5 (t_{2g})$  components are built on it.

Based on the above discussion, assignments of  $\nu_2 (e_g)$  and  $\nu_5 (t_{2g})$  JT-split transitions can be made independently of the assignments made for the electronic Raman spectra. The vibrations  $\nu_4 (t_{1u})$ ,  $\nu_5 (t_{2g})$ , and  $\nu_6 (t_{2u})$  are the bending vibrations ( $200\text{-}300 \text{ cm}^{-1}$ );  $\nu_4$  and  $\nu_6$  have been assigned. Thus, the six remaining major features in the bending region may be taken as components of  $\nu_5$ . The transitions in the bending mode combination region ( $400\text{-}600 \text{ cm}^{-1}$ , Figure 5) are of particular interest since no signals above background were observed in the electronic Raman spectrum. Most of these are assigned as  $2\nu_5$  components (see Table 2) because the various ( $\nu_4$ ,  $\nu_5$ ,  $\nu_6$ ) combinations and ( $\nu_4$ ,  $\nu_6$ ) overtones do not account for the observed number of peaks. (However, see discussion below as  $\nu_2 (J_2 = 3/2)$  states overlap this region.)

Assignments in the stretching region ( $600\text{-}700 \text{ cm}^{-1}$ ) can also be made. The transitions at  $685.8$  and  $692.0 \text{ cm}^{-1}$  do not have normal crystal field partners ( $34.6 \text{ cm}^{-1}$  to higher energy) and thus can be identified as  $\nu_2$  components. Two of the features at ca.  $600 \text{ cm}^{-1}$  are the  $J_2 = 3/2$  components of  $\nu_2$  based on a comparison with the electronic Raman spectrum.

A comparison between the electronic Raman and absorption data is made in Table 3. Since most assignments were made independently, their overall agreement adds strength to the interpretation. The small differences observed can be explained as either due to uncertainties in the electronic Raman data caused by poor signal-to-noise ratio (e.g.,  $\nu_5^1 (J_5 = 3/2)$ ) or differences in two-particle transition intensity patterns due to selection rules. As an example of the latter, compare the  $\sim 250 \text{ cm}^{-1}$   $\nu_5$  component in absorption (Figure 4) and electronic Raman scattering (Figure 2).

A theoretical understanding of the observed  $\nu_2$  and  $\nu_5$  JT-split vibrations is necessary in order to make more detailed assignments or extract parameter

values. It is probable that a coupled  $\nu_2$ - $\nu_5$  quadratic JT parametric calculation would meet these needs; however, the secular matrix for this difficult problem has not as yet been determined. Nonetheless, some of the above goals can be achieved by employing the presently available theoretical tools:  $\nu_2$ - $\nu_5$  linear JT secular matrix and GVC theory.<sup>(1)</sup> Examination of the data indicates that the  $\nu_2$  and  $\nu_5$  components appear in groups. The centers-of-gravity of these groups (Table 4) suggest the pattern expected for a linear JT effect. Thus, the data indicate that the linear coupling parameters,  $D_2$  and  $D_5$ , are larger than the quadratic terms. The  $\nu_2$ - $\nu_5$  linear JT calculation can be employed to assign to the above groups of peaks the appropriate linear JT quantum numbers ( $J_2$  or  $J_5$ ) and also to obtain rough parameter values. The linear parameters  $D_2$  and  $D_5$  are determined explicitly in the coupled linear calculation. While they can generate the appropriate splitting between major line groupings ( $J_i = 3/2$  and  $J_i = 1/2$ ), an accurate center-of-gravity for the entire pattern is not obtained. An acceptable fit to the overall  $\nu_2$  and  $\nu_5$  patterns comes about with introduction of totally symmetric quadratic parameters  $Q_i$  [ $a_{1g}$ ]. The effect of these particular quadratic terms in the Hamiltonian is to shift the center-of-gravity of the entire pattern by changing the apparent unperturbed vibrational frequency  $\nu_i^0$ . The parameters which are varied are: ( $D_2$ ,  $\nu_2^0$  ( $Q_2$  [ $a_{1g}$ ]),  $D_5$ ,  $\nu_5^0$  ( $Q_5$  [ $a_{1g}$ ])) with  $\nu_i^0$  ( $Q_i$  [ $a_{1g}$ ]) =  $\nu_i^0 \sqrt{1 + Q_i$  [ $a_{1g}$ ]}<sup>(1)</sup>. The  $\nu_i^0$  are determined by comparison with other non-JT perturbed states. In this case,  $\nu_5^0$  ~275  $\text{cm}^{-1}$  and  $\nu_2^0$  ~645  $\text{cm}^{-1}$ . The results of the calculation are given in Table 4 and have been used in the assignments in Tables 1-3. The rough parameter values obtained are:

$$D_5 = 0.13$$

$$Q_5$$
 [ $a_{1g}$ ] = -0.14,  $\nu_5^0$  ( $Q_5$  [ $a_{1g}$ ]) = 255  $\text{cm}^{-1}$

$$D_2 = 0.03$$

$$Q_2$$
 [ $a_{1g}$ ] = -0.04,  $\nu_2^0$  ( $Q_2$  [ $a_{1g}$ ]) = 630  $\text{cm}^{-1}$

Within the framework of a coupled  $v_2-v_5$  quadratic system, the  $\Gamma_5$  and  $\Gamma_7$  components account for all apparent shifts in centers-of-gravity of observed splitting patterns.

The GVC theory can be used to test the consistency of the interpretation since it predicts the number of components a given linear JT level generates under the action of higher order terms. It is also necessary to consider the effect of a low symmetry electronic crystal field on these levels. The  $\Gamma_5$  and  $\Gamma_7$  vibronic levels are Kramers doublets and are not split by macroscopic interactions, whereas  $\Gamma_{8g}$  level is split into two Kramers doublets by a low symmetry electrostatic field. A prediction of the number of components arising from each linear JT level can be made:

$$\begin{aligned} v_5 (J_5 = 3/2) &- 4 \\ v_5 (J_5 = 1/2) &- 2 \\ 2v_5 (J_5 = 5/2) &- 6 \\ 2v_5 (J_5 = 1/2) &- 2 \\ 2v_5 (J_5 = 3/2) &- 4 \\ v_2 (J_2 = 3/2) &- 2 \\ v_2 (J_2 = 1/2) &- 2. \end{aligned}$$

These predictions are well borne out by the data except where  $\Gamma_5$  and  $\Gamma_7$  overlap and  $v_2 (J_2 = 3/2)$  overlap. Five of the expected six transitions are found, but since the peaks are broad ( $\approx 10 \text{ cm}^{-1}$ ) it is possible that a near coincidence of peaks interferes with observation of the complete spectrum (see Figure 2).

It is interesting that all possible  $v_2$  and  $v_5$  components are observed. GVC theory predicts that only  $\Gamma_{8g}$  vibronic states should have intensity in absorption. Apparently other intensity mechanisms, such as Fermi resonance or vibronic coupling which is allowed by the  $C_5$  site symmetry, are important. An additional example of one of these alternative intensity mechanisms being operative is

found in the near IR absorption spectrum of  $\text{ReF}_6$  in which the  $(\Gamma_{7g} + \nu_5) \leftarrow \Gamma_{8g}$  transition has much more intensity than expected.<sup>(1)</sup> It should be noted that previous work on the  $\Gamma_{8g} ({}^2T_{1g})$  state of  $\text{IrF}_6$ <sup>(4)</sup> was hindered by lack of information in this regard; it had to be assumed that all  $\nu_5$  or  $\nu_2$  transitions were to a limited set of vibronic states ( $J_2 = J_5 = 1/2$  in linear JT theory).

The other quadratic parameters ( $Q_5 [e_g]$ ,  $Q_5 [t_{2g}]$ ,  $Q_2 [e_g]$ ) are not quantitatively obtained by this method, but qualitatively it is clear that their effect is substantial. For example, the  $\nu_5$  ( $J_5 = 3/2$ ) linear JT level is split by  $50 \text{ cm}^{-1}$  by these quadratic terms whereas the splitting of the  $\nu_5$  ( $J_5 = 3/2$ ) -  $\nu_5$  ( $J_5 = 1/2$ ) levels induced by linear JT terms is only  $\sim 100 \text{ cm}^{-1}$  (see Table 4). Thus, the conclusion reached previously<sup>(1,2)</sup> that the linear JT theory does not adequately describe the JT interactions observed in metal hexafluorides is strongly supported by these data.

A comparison of the JT behavior of the  $\Gamma_{8g} ({}^2T_{1g})$  ( $1.6 \mu$ ) state of  $\text{IrF}_6$  with that of the  $\Gamma_{8g}$  of  $\text{ReF}_6$ <sup>(1)</sup> and the  $\Gamma_{8g} ({}^2T_{2g})$  ( $0.6 \mu$ ) state of  $\text{IrF}_6$ <sup>(2)</sup> is of interest. The parameters which can be compared are:  $D_5$ ,  $Q_5 [a_{1g}]$ , ( $Q_5 [e_g]$ ,  $Q_5 [t_{2g}]$ ),  $D_2$ ,  $Q_2 [a_{1g}]$ ,  $Q_2 [e_g]$ . ( $Q_5 [e_g]$ ,  $Q_5 [t_{2g}]$ ) represents the combined effect of the two terms.

A comparison of the parameters is as follows:

$$\text{IrF}_6 (\Gamma_{8g} ({}^2T_{1g}) - 1.6 \mu) \text{ vs. } \text{IrF}_6 (\Gamma_{8g} ({}^2T_{2g}) - 0.6 \mu)$$

$$D_5^{1.6\mu} > D_5^{0.6\mu}$$

$$Q_5^{1.6\mu} [a_{1g}] < Q_5^{0.6\mu} [a_{1g}]$$

$$(Q_5^{1.6\mu} [e_g], Q_5^{1.6\mu} [t_{2g}]) > (Q_5^{0.6\mu} [e_g], Q_5^{0.6\mu} [t_{2g}])$$

and

$$\underline{\text{IrF}_6 (\Gamma_8 (^2T_{1g})) \text{ vs. } \text{ReF}_6 (\Gamma_{8g})}$$

$$D_5^{1.6\mu} \sim D_5^{\text{ReF}_6}$$

$$Q_5^{1.6\mu} [a_{1g}] \sim Q_5^{\text{ReF}_6} [a_{1g}]$$

$$(Q_5^{1.6\mu} [e_g], Q_5^{1.6\mu} [t_{2g}]) > (Q_5^{\text{ReF}_6} [e_g], Q_5^{\text{ReF}_6} [t_{2g}])$$

$$D_2^{1.6\mu} > D_2^{\text{ReF}_6}$$

$$Q_2^{1.6\mu} [a_{1g}] < Q_2^{\text{ReF}_6} [a_{1g}]$$

$$Q_2^{1.6\mu} [e_g] \sim Q_2^{\text{ReF}_6} [e_g].$$

One can conclude from this summary of vibronic parameters that the combined  $(Q_5^{1.6\mu} [e_g], Q_5^{1.6\mu} [t_{2g}])$  terms are the largest ones of this type. Moreover, they are larger than  $Q_5^{1.6\mu} [a_{1g}]$ , which is the opposite of the behavior seen in the other states.

A comparison of other JT-related characteristics of the two  $\text{IrF}_6$  states is also helpful. The  $\nu_5$  components of the  $\Gamma_{8g} (^2T_{2g})$  state are found to preserve the low-symmetry electronic crystal field splitting observed at the origin<sup>(2)</sup>, while in the present case, the crystal field splittings of  $\nu_5$  components are quenched to some extent. For example, the  $\nu_5$  ( $J = 1/2$ ) state is split by  $26.7 \text{ cm}^{-1}$  instead of the  $34.6 \text{ cm}^{-1}$  that the origin is split. Such behavior is consistent with the magnitudes of the  $D_5$  parameters ( $D_5^{1.6\mu} = 0.13$ ,  $D_5^{0.6\mu} = 0.03$ ) and the assumption that  $\text{IrF}_6$  experiences a crystal field of approximately  $D_{4h}$  symmetry.<sup>(2)</sup> As pointed out in Reference 1, in this case the  $\nu_5$  components approximately carry the origin splitting, but the approximation improves as  $D_5$  decreases. The JT activity of  $\nu_2$  in the  $\Gamma_{8g} (^2T_{1g})$  state

might also contribute to the different crystal field behavior; under these conditions an admixture of  $\nu_2$  character into the  $\nu_5$  levels would cause partial crystal field quenching.<sup>(1)</sup> Large quadratic terms such as ( $Q_5^{1.6\mu}[e_g]$ ,  $Q_5^{1.6\mu}[t_{2g}]$ ) might also contribute to this quenching. Another observation consistent with  $D_5^{1.6\mu} > D_5^{0.6\mu}$  is that the intensity in the  $2\nu_5$  region is significantly greater for the  $1.6\mu$  transition ( $\Gamma_{8g} ({}^2T_{1g})$ ).

Finally, the different crystal field behavior for  $\nu_5$  observed in different  $\Gamma_8$  states of  $\text{IrF}_6$  and  $\text{ReF}_6$  supports the contention that it is the molecular JT effect that dominates the distortion and not the low symmetry crystal field. It is therefore suggested that these data and conclusions should in general apply to the free  $O_h$  symmetry molecule.

#### IV. CONCLUSION

Absorption and electronic Raman spectroscopy have been used to elucidate the Jahn-Teller interaction in the  $\Gamma_{8g} (^2T_{1g})$  state at  $1.6\mu$  of  $\text{IrF}_6$ . As was found previously<sup>(1,2)</sup> for the  $\Gamma_8 (^2T_{2g})$  state of  $\text{IrF}_6$  and the ground  $\Gamma_8$  state of  $\text{ReF}_6$ , linear JT theory inadequately describes the experimental observations. In this case, however, different quadratic terms are found to be dominant, i.e.,  $(Q_5^{1.6\mu} [e_g], Q_5^{1.6\mu} [t_{2g}]) > Q_5^{1.6\mu} [a_{1g}]$ . Both quadratic and crystal effects relax the strict linear JT optical selection rules such that all possible transitions to JT active vibronic components are observed.

# REFERENCES

1. G. R. Meredith, J. D. Webb, E. R. Bernstein, Mol. Phys., 34, 995 (1977).
2. E. R. Bernstein, J. D. Webb, Mol. Phys., in press.
3. E. R. Bernstein, G. R. Meredith, J. D. Webb, J. Chem Phys., in press.
4. J.C.D. Brand, G. L. Goodman, B. Weinstock, J. Mol. Spec. 37, 464 (1971).
5. E. R. Bernstein, G. R. Meredith, J. Chem. Phys. 64, 375 (1976).
6. J. A. Koningstein, Introduction to the Theory of the Raman Effect (Reidel, Holland, 1972).
7. M. S. Child, H. C. Longuet-Higgins, Phil. Trans. Roy. Soc. 254A, 259 (1961).
8. E. R. Bernstein, G. R. Meredith, Chem. Phys. 24, 289-299, 301-309, 311-325 (1977).

Table 1. Electronic Raman spectrum of the  $\Gamma_{8g}$  ( $^2T_{1g}$ ) state of  $\text{IrF}_6$  in a  $\text{MoF}_6$  host crystal at a bath temperature of 1.6 K. The slit widths correspond to about  $10 \text{ cm}^{-1}$ ; the intense lines can be measured with an uncertainty of  $\pm 1 \text{ cm}^{-1}$  whereas the weaker lines are only accurate to  $\pm 3 \text{ cm}^{-1}$ .

$\sigma \text{ (cm}^{-1}\text{)}^{(a)}$ Vacuum	$\Delta\sigma \text{ (cm}^{-1}\text{)}$	I (b)	FWHH (c) $\text{(cm}^{-1}\text{)}$	Assignment (d)
6110	0	4000	10	Origin (a)
6138	28	3200	12	Origin (b)
6298	188	30	10	} $\nu_5 (J_5 = 3/2); \nu_4 (a, h)$
6343	233	25	--	
6363	253	60	30	
6423	313	45		$\nu_5 (J_5 = 1/2)$
6431	321	55		$\nu_5 (a, h)$
6445	335	50		$\nu_5 (J_5 = 1/2)$
6692	582	50	}	$\nu_2 (J_2 = 3/2)$
6705	595	60		
6796	686	280	}	$\nu_2 (J_2 = 1/2)$
6805	695	320		
6831	721	30		$\nu_3 (a, h)$

(a) Stokes shift from exciting laser line (either 5400 or 5500 Å).

(b) Approximate number of photon counts per second under the experimental conditions (see Section II).

(c) FWHH = full width at half height.

(d) The notation  $\nu_i (a, h)$  implies that  $\nu_i$  of the host ( $\text{MoF}_6$ ) is built on origin (a).

Table 2. Absorption spectrum of the  $\Gamma_{8g}$  ( $^2T_{1g}$ ) state of  $\text{IrF}_6/\text{MoF}_6$  at 1.6 K. Frequencies are given in vacuum wavenumbers and are accurate to  $\pm 0.1 \text{ cm}^{-1}$  for sharp lines.

$\sigma \text{ (cm}^{-1}\text{)}$ Vacuum	$\Delta\sigma \text{ (cm}^{-1}\text{)}$	I (a)	FWHH <sup>(b)</sup> (cm <sup>-1</sup> )	Assignment <sup>(c)</sup>
6109.6 (16363.3 Å)	0.0	M	$\leq 0.6$	Origin (a)
6144.2	34.6	S	2.5	Origin (b)
6305.0	195.4	M	1.6	$\nu_5^1$ ( $J_5 = 3/2$ )
6312.2	202.6	S	2.4	$\nu_6$ (a)
6322.8	213.3	W	1.6	$\nu_5^2$ ( $J_5 = 3/2$ )
6344.6	235.1	S	1.6	$\nu_5^3$ ( $J_5 = 3/2$ )
6346.9	237.4	S	1.6	$\nu_6$ (b)
6355.3	245.7	S	5.6	$\nu_5^4$ ( $J_5 = 3/2$ )
6365.4	255.8	W		} $\nu_4$ (a, h)
6373.1	236.6	W		
6377.0	267.4	W		
6389.8	280.3	W		
6394.4	284.9	M	2.8	$2\nu_6$ (a, h)
6400.7	291.1	S	4.0	$\nu_4$ (a)
6422.0	312.5	M	2.4	$\nu_5^5$ (a) ( $J_5 = 1/2$ ) <sup>(d)</sup>
6428.0	318.4	M	} 10.0 }	$\nu_4$ (b), $\nu_5$ (a, h)
6430.3	320.8	M		
6448.8	339.2	M	2.8	$\nu_5^6$ ( $J_5 = 1/2$ ) <sup>(d)</sup>
6510.4	400.9	W		
6516.9	407.3	W		$2\nu_6$
6527.6	418.0	W		

Table 2. (continued)

$\sigma$ (cm <sup>-1</sup> ) Vacuum	$\Delta\sigma$ (cm <sup>-1</sup> )	I (a)	FWHH <sup>(b)</sup> (cm <sup>-1</sup> )	Assignment <sup>(c)</sup>
6534.6	425.1	W		
6544.2	434.6	W	2.7	} $2\nu_5$ ( $J_5 = 5/2$ )
6551.3	441.8	W	2.7	
6558.0	448.5	W	12.0	
6562.3	452.7	W		
6575.0	465.5	W		
6581.7	472.2	W	8.0	
6595.6	486.0	W		$(\nu_6 + \nu_4)$ (a)
6621.2	511.7	W		
6626.5	517.0	W		$(\nu_6 + \nu_4)$ (b)
6637.1	527.5	M	15.0	} $2\nu_5$ ( $J_5 = 1/2$ ) <sup>(d)</sup>
6664.8	555.2	W	10.0	
6673.3	563.7	W		
6689.6	580.0	W		$\nu_2$ ( $J_2 = 3/2$ )
6700.0	590.5	W		$2\nu_5$ ( $J_5 = 3/2$ )
6706.5	596.9	W	17.0	$\nu_2$ ( $J_2 = 3/2$ )
6716.7	607.1	W		$2\nu_5$ ( $J_5 = 3/2$ )
6726.3	616.7	W	13.0	$2\nu_5$ ( $J_5 = 3/2$ )
6755.8	646.2	W		
6766.7	657.1	W		
6788.9	679.4	W		
6795.4	685.8	W	4.3	} $\nu_2$ ( $J_2 = 1/2$ )
6801.6	692.0	M	1.6	
6809.9	700.4	M	4.8	$\nu_1(a)$
6819.4	709.8	W		} $\nu_3(a,h)$

Table 2. (continued)

$\sigma$ (cm <sup>-1</sup> ) Vacuum	$\Delta\sigma$ (cm <sup>-1</sup> )	I (a)	FWHH <sup>(b)</sup> (cm <sup>-1</sup> )	Assignment <sup>(c)</sup>
6842.9	733.4	W	9.0	$\nu_1(b)$ ; $\nu_3(b,h)$
6876.4	766.8	W		
6888.8	779.2	W		
6894.2	784.7	W		
6988.4	878.8	W		
7003.0	893.5	W	15.0	$(\nu_1 + \nu_5^1)$ (a)
7016.0	906.4	W	14.0	$(\nu_1 + \nu_6)$ (a)
7025.9	916.2	W		$(\nu_1 + \nu_5^2)$ (a)

(a) Relative intensities: S = strong, M = medium, W = weak.

(b) FWHH = full width at half-height.

(c) The notation  $\nu_i$  (a) means the  $\nu_i$  mode built on the (a) origin.  $\nu_i$  (b) implies  $\nu_i$  built on origin (b).  $\nu_i$  (a,h) means that mode  $\nu_i$  of the host (MoF<sub>6</sub>) is built on origin (a). These latter two-particle transitions are discussed in more detail in references 1, 2, and 5.

(d) In GVC theory (see text) these levels can be identified as components of  $\Gamma_{8g}$  vibronic states.

Table 3. A Comparison of Absorption and Electronic Raman Data.

Electronic Raman	Absorption	Assignments
188	195.4	$\nu_5$ ( $J_5 = 3/2$ )
	213.3	
233	235.1	
253	245.7 <sup>(a)</sup>	
313	312.5	$\nu_5$ ( $J_5 = 1/2$ )
335	339.2	
582	580.0	$\nu_2$ ( $J_2 = 3/2$ )
595	596.9	
686	685.8	$\nu_2$ ( $J_2 = 1/2$ )
695	692.0	

(a) Region congested by presence of host-related features. (See text for discussion and Tables 1 and 2.)

Table 4. Comparison of a  $\nu_2$ - $\nu_5$  linear Jahn-Teller (LJT) calculation<sup>(1)</sup> with centers-of-gravity of various groups of experimentally observed transitions (see Table 2). The parameter values in the calculation are the following:  
 $D_5 = 0.13$ ,  $\nu_5^0 (Q_5 [a_{1g}]) = 255 \text{ cm}^{-1}$ ,  $D_2 = 0.03$ ,  $\nu_2^0 (Q_2 [a_{1g}]) = 630 \text{ cm}^{-1}$ .

LJT Level	$E_{\text{Calc}} (\text{cm}^{-1})$	$E_{\text{LJT}}^{(a)} (\text{cm}^{-1})$	$E_v^{(c)} (\text{cm}^{-1})$
$\nu_5 (J_5 = 3/2)$	218	220(50)	252
$\nu_5 (J_5 = 1/2)$	319	312 <sup>(b)</sup>	
$2\nu_5 (J_5 = 5/2)$	442	452(38)	515
$2\nu_5 (J_5 = 1/2)$	509	527 <sup>(b)</sup>	
$2\nu_5 (J_5 = 3/2)$	584	604(27)	
$\nu_2 (J_2 = 3/2)$	603	587(17)	638
$\nu_2 (J_2 = 1/2)$	696	689 <sup>(b)</sup>	

(a) Centers-of-gravity of various groups of  $\nu_5$  and  $\nu_2$  components; these approximate the LJT levels which would be observed in the absence of quadratic JT splitting. The parenthetical numbers are the maximum quadratic splitting.

(b) The lower component of the split  $\Gamma_8$  vibronic state is used here since the splitting can be identified as a crystal field splitting rather than as quadratic JT. The weight factor of the state is then doubled in the averaging process.

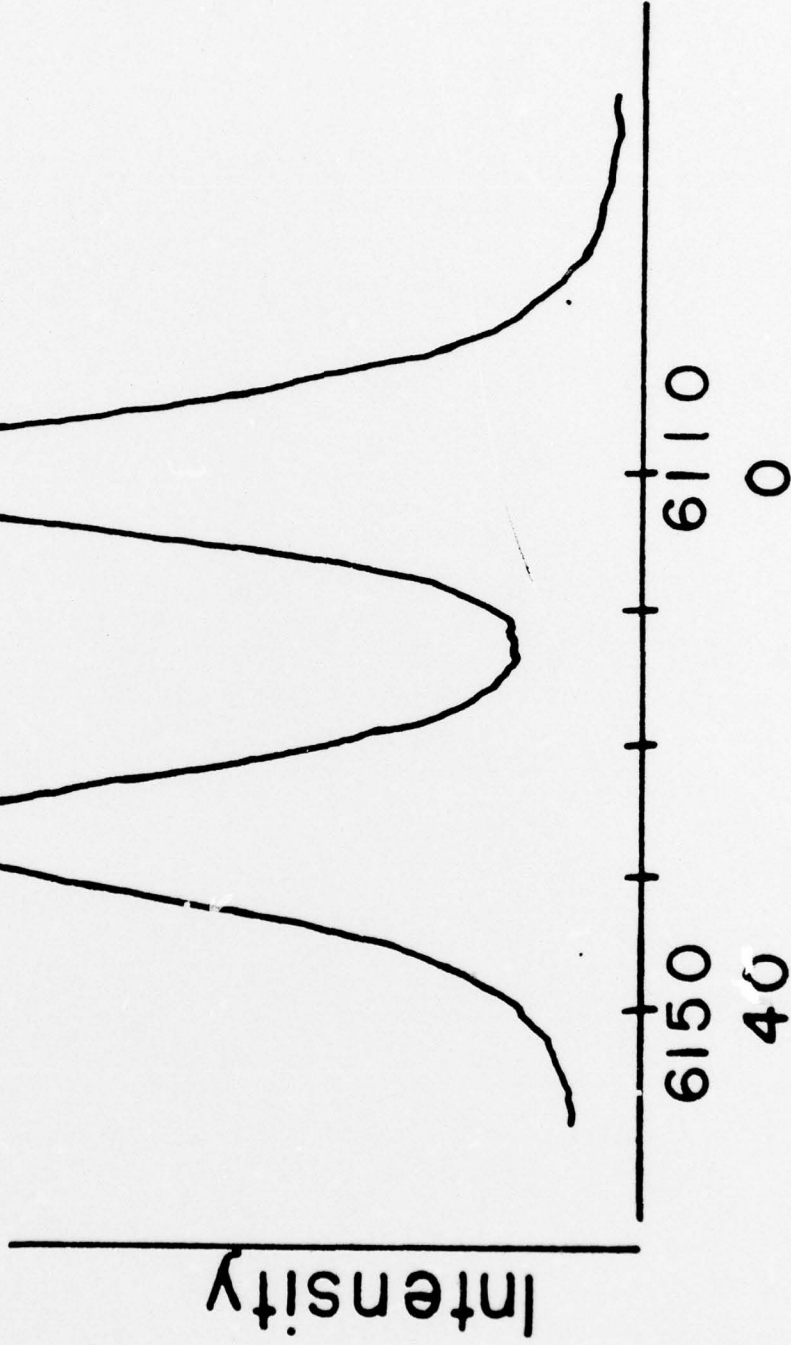
(c) Centers-of-gravity of the LJT levels.

Figure 1.

Origin region of  $\Gamma_{8g}$  ( $^2T_{1g}$ ) state of  $\text{IrF}_6/\text{MoF}_6$  as observed in electronic Raman scattering. The two peaks are components of the  $\Gamma_{8g}$  state which is split by a low symmetry crystal field.

5%  $\text{IrF}_6/\text{MoF}_6$

Origin ( $\Gamma_8(2T_1)$ )



Stokes Shift -  $\text{cm}^{-1}$

$\Delta E(\text{Origin } \Gamma_8(2T_1)) - \text{cm}^{-1}$

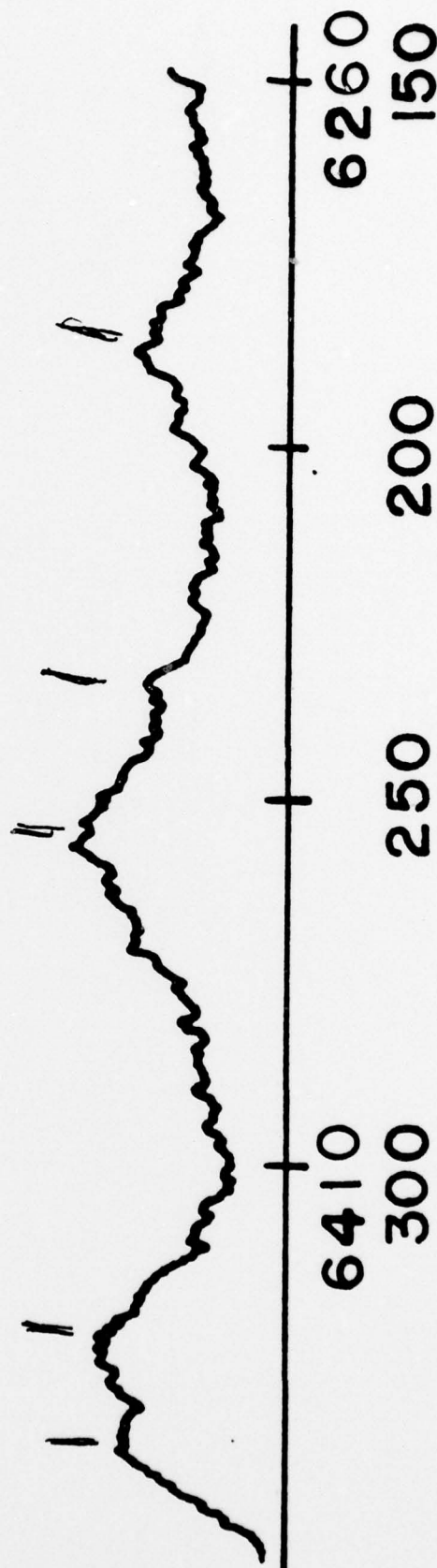
Figure 2.

The electronic Raman spectrum of the vibrational bending region of the  $\Gamma_{8g}$  ( $^2T_{1g}$ ) electronic state of  $\text{IrF}_6/\text{MoF}_6$ . These peaks are identified as Jahn-Teller-split  $\nu_5$  ( $t_{2g}$ ) components. Tables 1 and 3 contain detailed assignments.

5%  $\text{IrF}_6/\text{MoF}_6$

$\nu_5(\Gamma_8(2T_1))$

Intensity



Stokes Shift -  $\text{cm}^{-1}$   
 $\Delta E$  (Origin  $\Gamma_8(2T_1)$ ) -  $\text{cm}^{-1}$

Figure 3.

The electronic Raman spectrum of the vibrational stretching region of the  $t_{8g} (^2T_{1g})$  electronic state of  $IrF_6/MoF_6$ . The main features are identified as  $\nu_2 (e_g)$  components. A slower scan, with higher time constant, of the feature at  $690\text{ cm}^{-1}$  shows that it consists of two components (see Table 1).

5%  $\text{IrF}_6/\text{MoF}_6$

$\nu_2(\Gamma_8(2T_1))$

Intensity

6810

700

650

600

6660

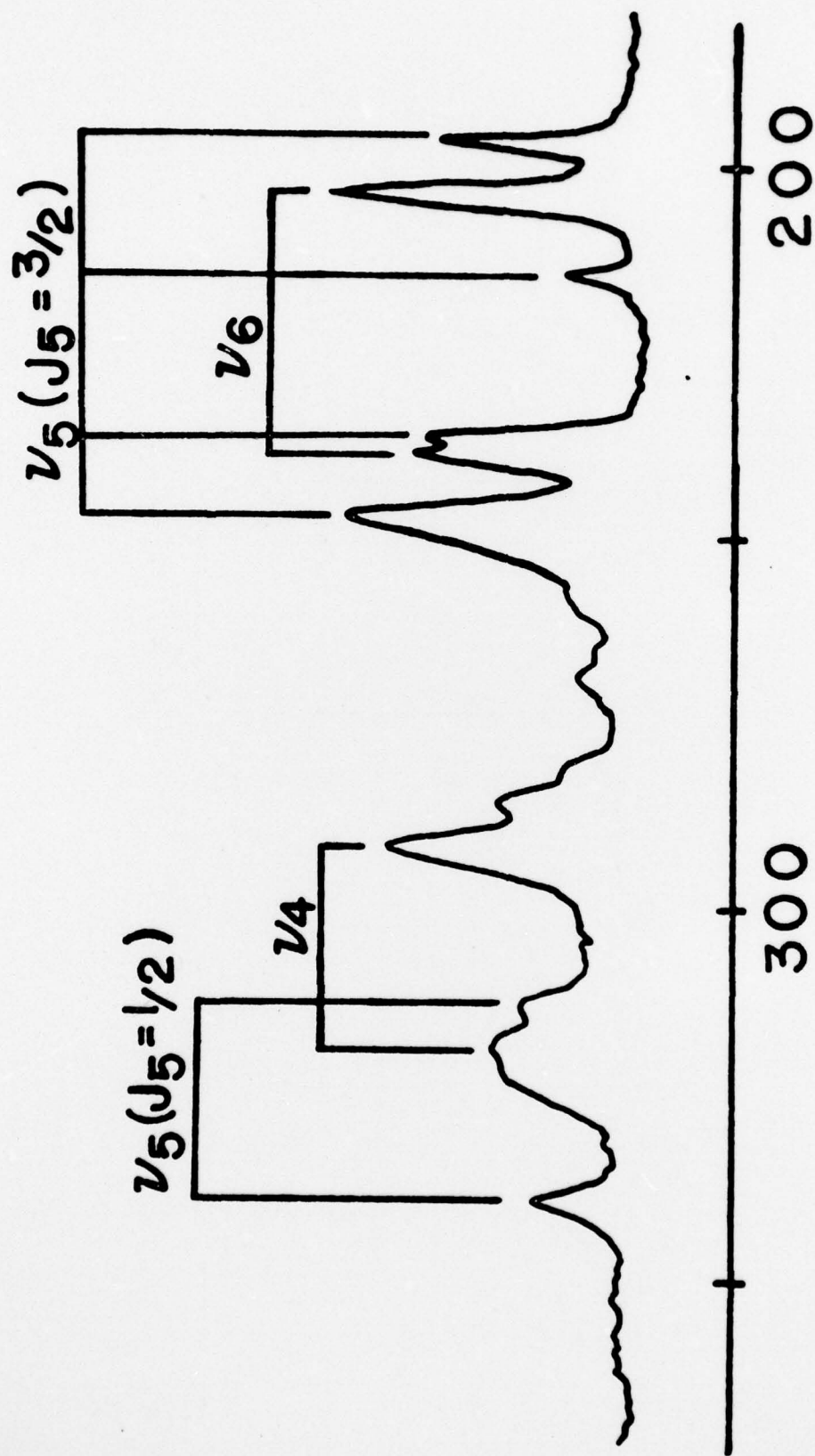
550

Stokes Shift -  $\text{cm}^{-1}$

$\Delta E(\text{Origin } \Gamma_8(2T_1)) - \text{cm}^{-1}$

Figure 4.

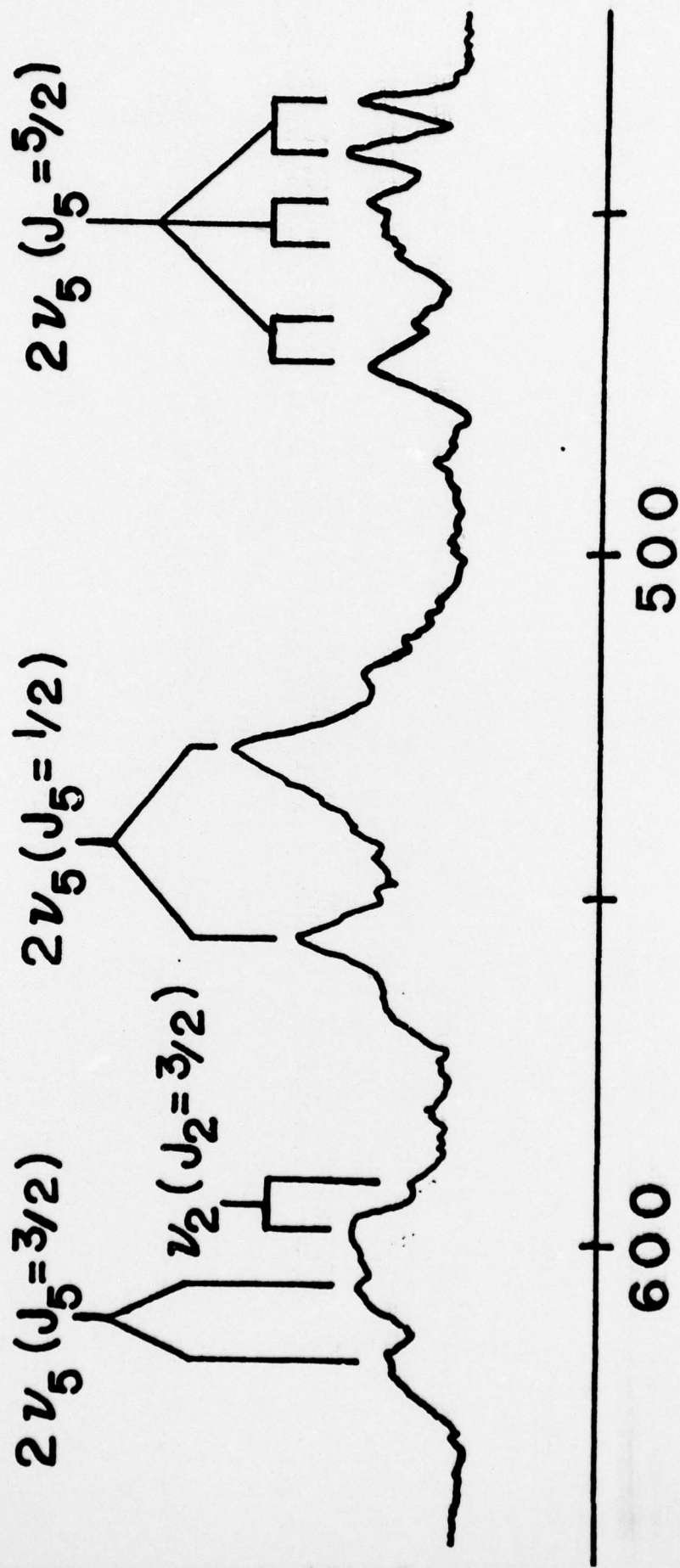
Absorption spectrum of the vibrational bending region of the  $\Gamma_{8g}$  ( $^2T_{1g}$ ) electronic state of  $\text{IrF}_6/\text{MoF}_6$ . Compare with the corresponding electronic Raman spectrum in Figure 2; the  $\nu_6$  and  $\nu_4$  features are absent there. Note that the  $\nu_5$  ( $n_5 = 1$ ) vibration is split by both a linear and quadratic Jahn-Teller effect. The linear term produces  $J_5 = 3/2$  and  $J_5 = 1/2$  levels, while the quadratic and low symmetry crystal field terms give the further splittings of these linear JT components.



$\Delta E$  (origin  $\Gamma_{8g}(^2T_{1g})$ ) /  $\text{cm}^{-1}$

Figure 5.

Absorption spectrum of the vibrational combination and overtone bending region in the  $\Gamma_{8g}$  ( $^2T_{1g}$ ) electronic state of  $\text{IrF}_6/\text{MoF}_6$ . Most of the features are identified as components of the Jahn-Teller active vibrations,  $\nu_2$  ( $e_g$ ) or  $\nu_5$  ( $t_{2g}$ ). Note the groupings of the peaks; these serve to identify the positions of the linear Jahn-Teller (LJT) levels in the absence of quadratic JT splitting. (See text and Table 4.)



$$\Delta E (\text{origin } \Gamma_{8g}(2T_{1g}))/\text{cm}^{-1}$$

Figure 6.

Absorption spectrum of  $\text{IrF}_6/\text{MoF}_6$  in the vibrational stretching region of the  $\Gamma_{8g} (^2T_{1g})$  electronic state of  $\text{IrF}_6/\text{MoF}_6$ . The splitting of the  $J_2 = 1/2$  component of  $\nu_2 (e_g)$  is caused by the low symmetry crystal field. Its value (about  $6 \text{ cm}^{-1}$ ) has been substantially reduced from the origin splitting by vibronic interaction.



$$\Delta E (\text{origin } \Gamma_{8g}(^2T_{1g}))/\text{cm}^{-1}$$

# TECHNICAL REPORT DISTRIBUTION LIST

## No. Copies

## No. Copies

Office of Naval Research  
Arlington, Virginia 22217  
Attn: Code 472

2

Office of Naval Research  
Arlington, Virginia 22217  
Attn: Code 1021P 1

6

ONR Branch Office  
536 S. Clark Street  
Chicago, Illinois 60605  
Attn: Dr. Jerry Smith

1

ONR Branch Office  
715 Broadway  
New York, New York 10003  
Attn: Scientific Dept.

1

ONR Branch Office  
1030 East Green Street  
Pasadena, California 91106  
Attn: Dr. R. J. Marcus

1

ONR Branch Office  
760 Market Street, Rm. 447  
San Francisco, California 94102  
Attn: Dr. P. A. Miller

1

ONR Branch Office  
495 Summer Street  
Boston, Massachusetts 02210  
Attn: Dr. L. H. Peebles

1

Director, Naval Research Laboratory  
Washington, D.C. 20390  
Attn: Code 6100

1

The Asst. Secretary of the Navy (R&D)  
Department of the Navy  
Room 4E736, Pentagon  
Washington, D.C. 20350

1

Commander, Naval Air Systems Command  
Department of the Navy  
Washington, D.C. 20360  
Attn: Code 310C (H. Rosenwasser) 1

Defense Documentation Center  
Building 5, Cameron Station  
Alexandria, Virginia 22314

12

U.S. Army Research Office  
P.O. Box 12211  
Research Triangle Park, N.C. 27709  
Attn: CRD-AA-IP

1

Naval Ocean Systems Center  
San Diego, California 92152  
Attn: Mr. Joe McCartney

1

Naval Weapons Center  
China Lake, California 93555  
Attn: Head, Chemistry Division

1

Naval Civil Engineering Laboratory  
Port Hueneme, California 93041  
Attn: Mr. W. S. Haynes

1

Professor O. Heinz  
Department of Physics & Chemistry  
Naval Postgraduate School  
Monterey, California 93940

1

Dr. A. L. Slafkosky  
Scientific Advisor  
Commandant of the Marine Corps (Code RD-1)  
Washington, D.C. 20380

1

Office of Naval Research  
Arlington, Virginia 22217  
Attn: Dr. Richard S. Miller

1

# TECHNICAL REPORT DISTRIBUTION LIST

	<u>No. Copies</u>		<u>No. Copies</u>
Dr. M. A. El-Sayed University of California Department of Chemistry Los Angeles, California 90024	1	Dr. G. B. Schuster University of Illinois Chemistry Department Urbana, Illinois 61801	1
Dr. M. W. Windsor Washington State University Department of Chemistry Pullman, Washington 99163	1	Dr. E. M. Eyring University of Utah Department of Chemistry Salt Lake City, Utah	1
Dr. E. R. Bernstein Colorado State University Department of Chemistry Fort Collins, Colorado 80521	1	Dr. A. Adamson University of Southern California Department of Chemistry Los Angeles, California 90007	1
Dr. C. A. Heller Naval Weapons Center Code 6059 China Lake, California 93555	1	Dr. M. S. Wrighton Massachusetts Institute of Technology Department of Chemistry Cambridge, Massachusetts 02139	1
Dr. M. H. Chisholm Princeton University Department of Chemistry Princeton, New Jersey 08540	1	Dr. M. Rauhut American Cyanamid Company Chemical Research Division Bound Brook, New Jersey 08805	1
Dr. J. R. MacDonald Naval Research Laboratory Chemistry Division Code 6110 Washington, D.C. 20375	1		